NANO LETTERS

2009
Vol. 9, No. 6
2267-2272

Synthesis, Electronic Structure, and Raman Scattering of Phosphorus-Doped Single-Wall Carbon Nanotubes

I. O. Maciel,[†] J. Campos-Delgado,[‡] E. Cruz-Silva,[§] M. A. Pimenta,[†] B. G. Sumpter,[§] V. Meunier,[§] F. López-Urías,[‡] E. Muñoz-Sandoval,[‡] H. Terrones,[‡] M. Terrones,[‡] and A. Jorio*[,†,||]

Departamento de Física, Universidade Federal de Minas Gerais, Belo Horizonte, MG, 31270-901 Brazil, Laboratory for Nanoscience and Nanotechnology Research (LINAN) & Advanced Materials Department, IPICYT, San Luis Potosí, SLP, Mexico, Oak Ridge National Laboratory, P.O. Box 2008 Oak Ridge, Tennessee 37830-6367, and Divisão de Metrologia de Materiais, Instituto Nacional de Metrologia, Normalização e Qualidade Industrial (INMETRO), Duque de Caxias, RJ, 25250-020, Brazil

Received February 9, 2009; Revised Manuscript Received April 30, 2009

ABSTRACT

Substitutional phosphorus doping in single-wall carbon nanotubes (SWNTs) is investigated by density functional theory and resonance Raman spectroscopy. Electronic structure calculations predict charge localization on the phosphorus atom, generating nondispersive valence and conduction bands close to the Fermi level. Besides confirming sustitutional doping, accurate analysis of electron and phonon renormalization effects in the double-resonance Raman process elucidates the different nature of the phosphorus donor doping (localized) when compared to nitrogen substitutional doping (nonlocalized) in SWNTs.

By doping single-wall (SWNT) and multiwall (MWNT) carbon nanotubes, it is possible to significantly change their physical and chemical properties, and this fact can be used for developing novel materials.[1−4] The most studied doped carbon nanotubes are those containing boron (B) and nitrogen (N).[5−8] B and N are the neighbors of carbon (C) in the periodic table that can provide p- and n-doping, respectively, their valence electrons being in the second shell, like carbon. Phosphorus (P) is another electron donor that can be incorporated into nanotubes, but fundamentally different from N because its valence electrons are in the third shell. Recent studies carried out using energy dispersive X-ray (EDX) and electron energy loss spectroscopy (EELS) have demonstrated that P and N can be homogeneously incorporated into the lattice of MWNTs (with diameters usually above 20 nm),[9] changing MWNTs chemical properties and morphology.[10−13] P atoms were also used to dope fullerenes for biological applications.[14] However, doping SWNTs with large contents of P is challenging because (i) this element reduces catalytic activity of Fe during nanotube growth and (ii) P atoms are larger than C atoms, thus increasing the disorder within the hexagonal carbon framework.[9] Besides these difficulties, the growth of SWNTs with low doping levels of P leads to new perspectives toward the control of SWNT electronic properties. In this work we report the successful synthesis of P-doped SWNTs, and we use density functional theory (DFT) and resonance Raman spectroscopy to explore their novel properties when compared to the usual donor-doping of N in SWNTs. Resonance Raman spectroscopy is employed here as a powerful tool to confirm substitutional doping and analyze changes in the electronic and vibrational structure. More specifically, the so-called G′ band, a strong double-resonance second-order Raman feature appearing around 2700 cm^{-1}, has been shown to be very sensitive to substitutional p- or n-type doping in SWNTs, even at small concentrations of boron and nitrogen doping (e.g., 0.3% at.),[15] and it will be discussed here in detail.

In order to explore the fundamental difference between the effect of P and N doping, electronic structure calculations were performed using density functional theory, as implemented in Siesta[16] and detailed in a previous publication.[9] The theoretically studied nanotubes consisted of pristine, N- and P-doped zigzag (10,0), (12,0), (15,0), and armchair (6,6), (8,8), (10,10) nanotubes. In order to avoid interactions of

* Corresponding author, adojorio@fisica.ufmg.br.
[†] Departamento de Física, Universidade Federal de Minas Gerais.
[‡] Laboratory for Nanoscience and Nanotechnology Research (LINAN) & Advanced Materials Department, IPICYT.
[§] Oak Ridge National Laboratory.
[||] Divisão de Metrologia de Materiais, Instituto Nacional de Metrologia, Normalização e Qualidade Industrial (INMETRO).

10.1021/nl9004207 CCC: $40.75
Published on Web 05/18/2009

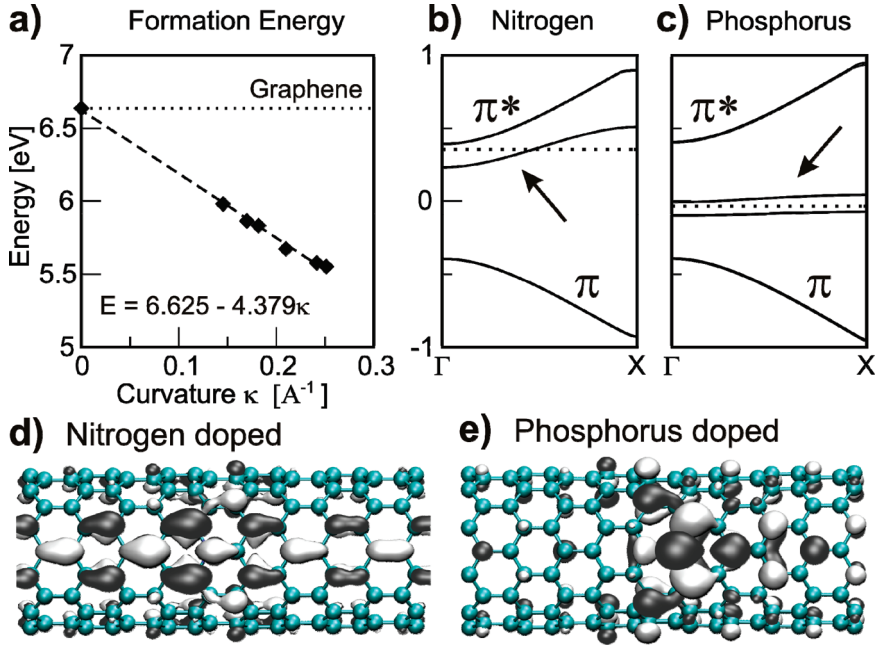

Figure 1. (a) Plot of defect formation energy vs curvature. Dotted line represents the formation energy for a planar graphene sheet, as the limit for large nanotubes. (b, c) Electronic band structure near Fermi level for (b) N- and (c) P-doped (10,0) nanotube. (d) and (e) Real space representations of the states marked by arrows in (b) and (c). It is evident that while the N state is distributed over the entire supercell, the P state is localized around the phosphorus atom. The strong localization in the phosphorus case is responsible for the dispersionless flat bands, which correspond to spin up and down states.

the doping atoms with their periodic images, supercells of eight repeating units (19.81 Å) were considered for armchair nanotubes, while five unit cells (21.52 Å) were considered for the zigzag cases.

The defect formation energy was computed from DFT, considering

$$\Delta E = E_D - E_{Pris} - \mu_P - \mu_C \quad (1)$$

where E_D (E_{Pris}) is the total energy for the P-doped (pristine) SWNT, and μ_P (μ_C) is the total energy of isolated P (C) atoms. These energies are plotted in Figure 1a, showing that the formation energy decreases as the curvature κ (inverse of the nanotube radius) increases, with a fitted relation ΔE (eV) $\sim 6.625 - 4.379\kappa$. This reduction reflects the lower strain in the carbon network required to accept the trigonal bonds of the phosphorus ion when the nanotube diameter is smaller. Therefore, phosphorus doping is more likely to occur in smaller diameter nanotubes and in fact can induce the formation of thinner nanotubes when doping occurs during growth.

Turning to their electronic properties, both P and N doping create new states associated with the presence of the doping atom, which appear close to the Fermi energy, as indicated by arrows in parts b and c in Figure 1 for a (10,0) nanotube. For N, this state lies beneath the conduction bands, shifting the Fermi energy and causing all N-doped nanotubes to be metallic. P creates a highly localized state that appears as a dispersionless flat band in the band structure, as seen in Figure 1c, which is projected as a set of sharp peaks in the electronic density of states around the Fermi level. Due to their localized nature, these P-related states do not contribute with electrons to the conduction bands, and therefore they do not affect the semiconductive or metallic character of the nanotubes. The presence of two nondispersive P-related bands, one in the valence and another in the conduction band, is related to the spin polarization. The splitting of about 0.1 eV within the local density approximation (LDA) and 0.25 eV within the generalized gradient approximation (GGA) is due to a higher exchange energy related to a greater spatial localization of the orbital. This type of unique electronic structure is a promising feature for solid-state-based quantum computer archtectures,[17] as previously shown for similar spin-based quantum computer architectures, such as P-doped Si substrates.[18]

The growth methods for doped nanotubes, in particular chemical vapor deposition (CVD)[6] and laser ablation,[5,7] lead to samples of good crystallinity and substitutional doping, as confirmed by EELS and EDX, especially for MWNTs.[4,9] For SWNTs, smaller amounts of doping have to be inserted into the growth environment in order to obtain samples of good crystallinity. It is therefore harder to detect the presence of dopants in SWNT samples since the doping level is typically below the detection sensitivity limits of most of the instruments available to date for the different elemental mapping techniques. The SWNTs doped with P studied here were grown by CVD at 950 °C using solutions of ethanol (C_2H_6O) with 1.25% by weight of ferrocene ($C_{10}H_{10}Fe$) and triphenylphosphine ($C_{18}H_{15}P$) as P precursor, at different concentrations. An aerosol of the solution was produced ultrasonically and then carried inside a quartz tube to the hot zone of a tubular furnace with a flow rate of 0.8 L/min of an Ar−H gas mixture (5% of hydrogen), during 30 min. After that time, the system was allowed to cool down to

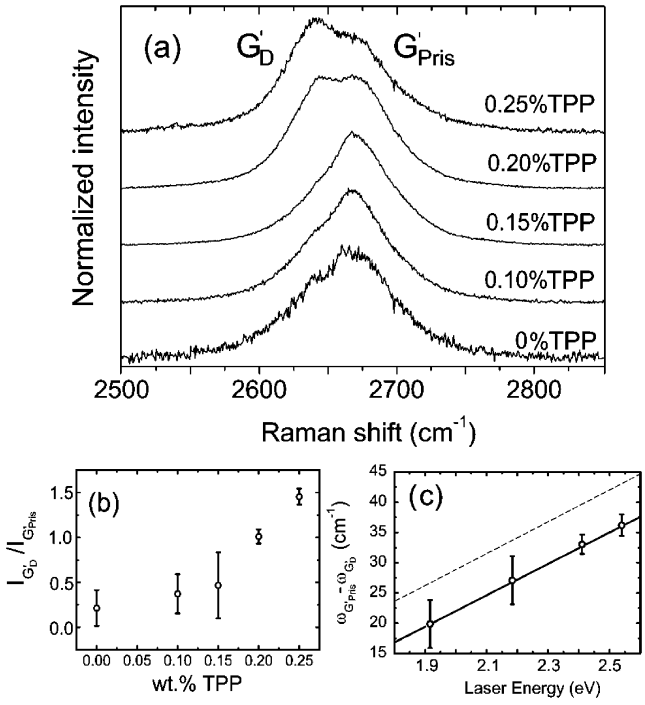

Figure 2. (a) G′ bands of phosphorus-doped samples, taken at low laser power (0.2 mW), after annealing the samples with 2 mW laser power (E_{Laser} = 2.41 eV). (b) $I_{G'_D}/I_{G'_{Pris}}$ relative intensity for the Raman spectra shown in (a). The error bars come from measurements in five different locations in the sample. (c) $\omega_{G'_{Pris}} - \omega_{G'_D}$ of the 0.2 wt % TPP-doped samples (symbols) as a function of the laser energy. The lines are the fits to the $\omega_{G'_{Pris}} - \omega_{G'_D}$ data from this work (solid line, $(26 \pm 1)E_{laser} - (30 \pm 1)$) and from ref 10 (N-doped samples, dashed line, $(24 \pm 4)E_{laser} - (19 \pm 8)$). The error bars reflect the frequency uncertainty to fit the peaks for the 0.2 wt % sample.

room temperature, maintaining a flow rate of 0.2 L/min of the same Ar−H gas mixture. Once the system was cold, the quartz tube was removed and the material of interest was collected from the walls as a web containing strands of bundles, following the procedure described in ref 6 for the CVD production of N-doped SWNTs. In the following discussion, the samples analyzed will be identified by the different concentrations of doping precursor inserted in the starting solution, which were 0%, 0.1%, 0.15%, 0.20%, and 0.25% by weight of triphenylphosphine (TPP), since the real percentage of P in the final material is not known.

In order to identify and study the P doping in SWNTs, Raman spectra were acquired with a Dilor XY triple-monochromator equipped with CCD detector in the back-scattering configuration, using an 80× objective. The Raman spectra from small diameter (d_t < 2 nm) SWNTs are known to be several orders of magnitude higher than other graphitic coproducts, due to its resonant nature.[19,20] Furthermore, the second-order G′ band frequency is highly sensitive to changes in the sp^2 carbon structures, including changes in tube diameter[19,21] and structural changes induced by doping.[15] For this reason, it is clear the Raman spectra we will discuss comes from doped SWNTs. Figure 2a shows a two-peak G′ feature of P-doped samples after annealing with 2 mW laser power. The spectra were taken with a laser excitation energy of 2.41 eV at a power of 0.2 mW. As discussed in ref 15, undoped samples exhibit a single peak G′ feature, named G'_{Pris} (Pris stands for pristine), while n-type doped tubes exhibit two G′ features: the G'_{Pris} and a red-shifted peak, named G'_D (D stands for doping), which is due to doping-induced electron and phonon renormalization near the doping sites.[15] The frequencies of the two G′ peaks do not change with increasing the doping level, meaning that the doped regions contain the same charge in all the samples and only their number increases with increasing doping concentration, thereby increasing the $I_{G'_D}/I_{G'_{Pris}}$ relative intensity between the two G′ peaks, as shown in Figure 2b. From Figure 2b, doping seems to be more effective above 0.15 wt %, since the $I_{G'_D}/I_{G'_{Pris}}$ relative intensity increases significantly above this doping level.

For deeper physical insights, we measured the frequencies of the G'_{Pris} and G'_D bands as a function of the excitation laser energy, thus accurately probing their resonant dispersive behavior. The symbols in Figure 2c stand for the $\omega_{G'_{Pris}} - \omega_{G'_D}$ frequency splitting between the two G′ peaks for the 0.2 wt % P-doped sample, which is a measure of the charge-induced electron and phonon energy normalization.[15] The dashed line is a fit of the $\omega_{G'_{Pris}} - \omega_{G'_D}$ behavior of a N-doped SWNT sample, taken from ref 15. The $\omega_{G'_{Pris}} - \omega_{G'_D}$ splitting is smaller for P when compared to N, yet the E_{laser} dispersion remaining the same for the two types of doping. Although a quantitative understanding of this effect requires the development of a double resonance model for doped SWNTs, this result is consistent with the theoretical finding that P-induced states have a higher spatial localization compared to N-induced states, hence causing a lower perturbation in the charge distribution, as shown in the real space representation of the P- and N-induced states of parts d and e of Figure 1.

Changes in the SWNT diameter distribution, the resonance conditions, nonlocal charge transfer, or heating effects can also cause Raman frequency shifts. Therefore, it is important to rule out any other effect that could be responsible for the differences in $\omega_{G'_{Pris}} - \omega_{G'_D}$. The $\omega_{G'}$ is known to depend on tube diameter (d_t).[19,21] The radial breathing mode (RBM), around 100−400 cm^{-1}, yields information about the d_t,[20,22−24] and mapping of the RBMs as a function of the excitation laser energy was performed with excitation energies ranging from 1.61 to 2.71 eV. An Ar−Kr laser (1.91, 2.18, 2.33, 2.41, 2.47, 2.49, 2.53, 2.60, 2.62, and 2.71 eV) and a dye tunable laser (16 lines from 1.80 to 2.01 eV; 16 lines from 2.03 to 2.19 eV and 5 lines from 2.23 to 2.29 eV) were used. The RBM peak position is related to the tube diameter by[22]

$$\omega_{RBM} = \frac{227}{d_t}\sqrt{1 + Cd_t^2} \qquad (2)$$

where ω_{RBM} is the RBM frequency shift in cm^{-1}, d_t is the tube diameter in nanometers, and C is a constant factor accounting for environmental effects.[22] By measuring the RBMs with different laser energies, it is possible to build a two-dimensional map of the RBM profiles as a function of the excitation laser energy.[22−25] Figure 3 shows such maps in the 1.9−2.3 eV energy range for the 0, 0.1, 0.15, 0.2, and 0.25 wt % of P-doped SWNT samples. The maps show the

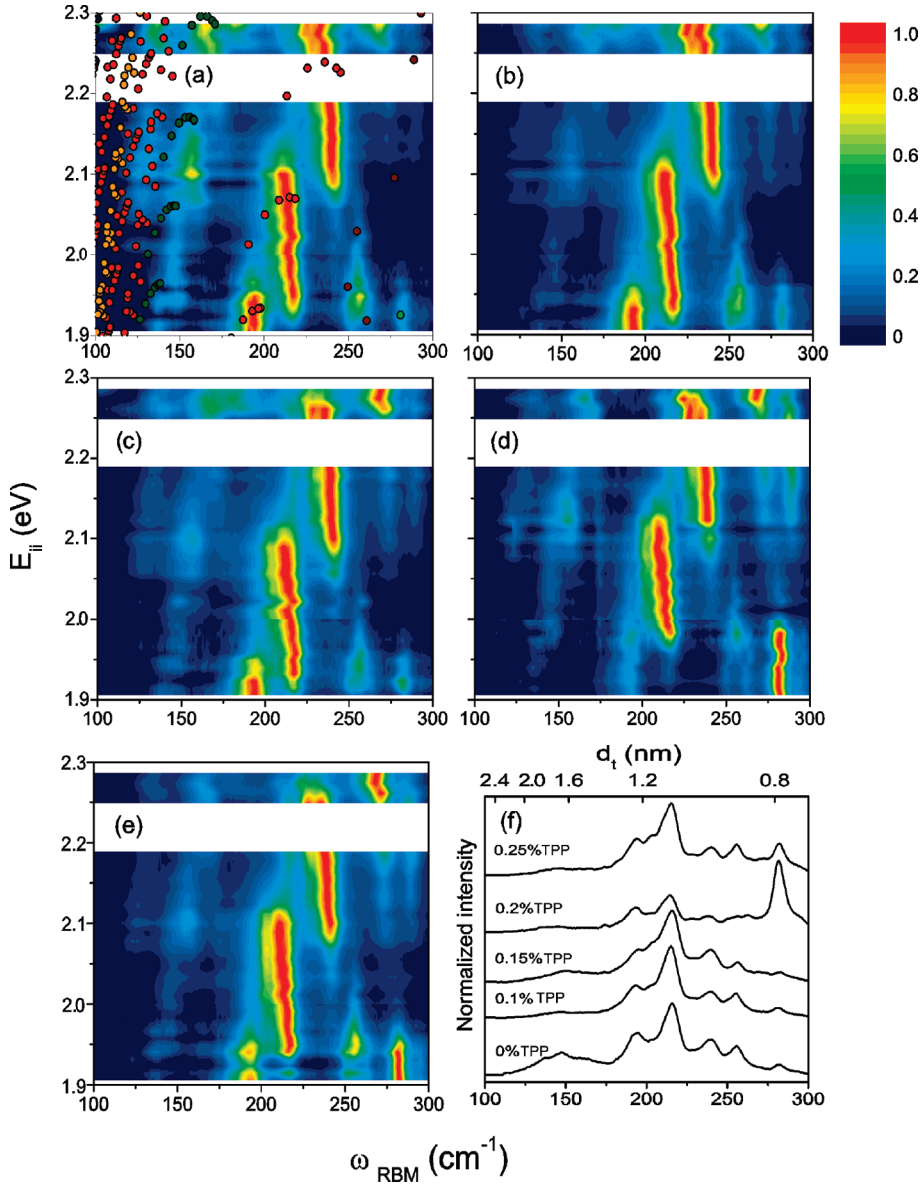

Figure 3. (a−e) Radial breathing mode (RBM) resonance Raman maps of the phosphorus-doped SWNT samples with 0, 0.1, 0.15, 0.2, 0.25 wt % of TPP, respectively. The optical transmission energies (E_{ii})[26] were inserted on the map of the undoped sample (a) to indicate the (n,m)-dependent RBM resonances by using eq 2,[22] with the best fit to our data given by $C = 0.035$. (f) Diameter distribution of the samples obtained by summing all the RBM spectra measured with the different excitation laser lines. The upper x-axis was obtained by the inverse of the $\omega_{RBM}-d_t$ relation cited above.

resonance patterns related to different $(2n + m) =$ constant families belonging to the E^{S}_{22}, E^{M}_{11}, E^{S}_{33}, transition energies, (n,m) being the nanotube indices.[22] No ω_{RBM} or optical transition energies (E_{ii}) shift can be seen from the maps upon different doping levels, thus indicating that the local nature of P doping does not change either ω_{RBM} or the E_{ii} of the SWNTs.

Although the RBM Raman cross section depends on (n,m) and E_{ii},[27−29] a qualitative description of the diameter distribution of the samples can be obtained by adding all the RBM spectra for each sample, as shown in Figure 3f. The diameters vary from 0.7 to 2.2 nm for the different samples. However, the samples with higher doping levels (0.2 wt % and 0.25 wt %) have larger RBM intensities with higher RBM frequencies, meaning that either the presence of P induces the formation of tubes with smaller diameters or the relative Raman scattering of narrower tubes has been enhanced by doping. In both cases, this result is in agreement with the conclusions taken from Figure 1a and, together with the two-peak G′ feature, they confirm substitutional phosphorus doping. Finally, this accurate information on the diameter distribution, based on the ω_{RBM} analysis, was used to analyze the $\omega_{G'}$ peaks and we can rule out any diameter or resonance effects as responsible for the behavior of the $\omega_{G'_{Pris}} - \omega_{G'_{D}}$ splitting. The change in the RBM intensity toward high ω_{RBM} frequencies above 0.15 wt % of TPP results indeed confirms the effect evidenced by the $\omega_{G'}$ analysis, where doping seems to be more effective above this doping level.

In addition, the $\omega_{G'_{Pris}} - \omega_{G'_{D}}$ effect can be related not to the localized vs nonlocalized nature of the doping but to different charge transfer or even temperature effects. In this context, the tangential (G^{+}) band in nanotubes, around 1590

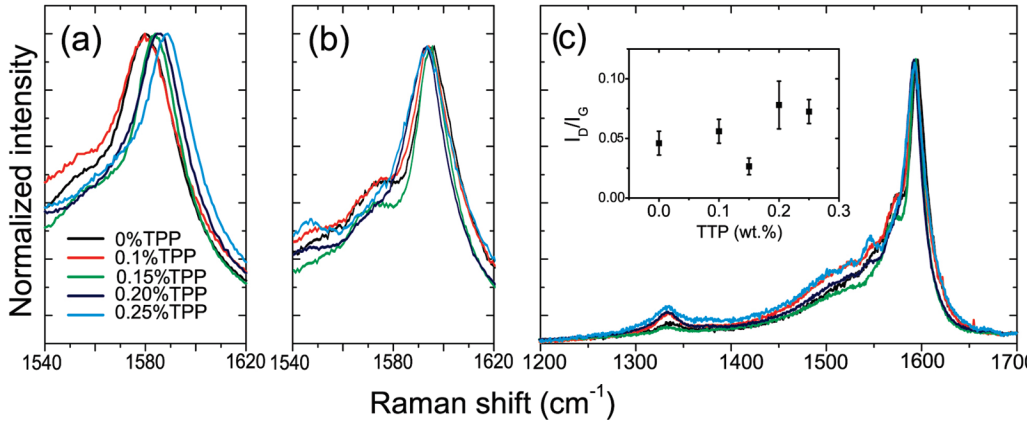

Figure 4. Tangential mode (G band) for phosphorus-doped samples measured with (a) 2 mW and (b) 0.2 mW at 2.41 eV. Different line colors indicate the doping levels (see Figure legend). The D band is evidenced in (c), where the spectra were measured with 0.2 mW. All the spectra are normalized to the G band intensity. The relative intensities I_D /I_G (see inset to c) remain always smaller than 0.1, showing (i) the good crystallinity of all samples and (ii) that this I_D /I_G ratio is not as accurate as the $I_{G'_D}/I_{G'_{Pris}}$ ratio (Figure 2b) to measure doping level.

cm^{-1}, is known to shift with gating amplitude[30] and interstitial[4,31,32] doping. Figure 4a shows a zoom at the G^+ band for P-doped samples measured with $E_{laser} = 2.41$ eV and 2 mW laser power, while Figure 4b depicts measurements made at 0.2 mW. At low laser power (Figure 4, panels b and c), the G^+ band frequency ω_{G^+} of all the doped samples is independent of doping. When the samples are measured at high laser power (Figure 4a), the frequencies of the different doped samples downshift differently with respect to the value measured with 0.2 mW laser power, ranging from 1578 to 1588 cm^{-1}. The sample with highest doping level exhibits the smallest red shift (-6 cm^{-1}), while the sample with the lowest doping level exhibits the largest red shift (-16 cm^{-1}). The downshifts are caused by laser-induced heating and the smaller ω_{G^+} downshift for the larger doping level indicates that P doping enhances the thermal conductivity of the sample. The substitutional P introduces strain, and it is likely that the grain boundary scattering enhances the inter-SWNT heat transfer in the SWNT bundles, important for thermoelectric applications.

In summary, we have demonstrated that SWNTs can be successfully doped with P and have carried out a detailed study of P-doped SWNTs properties by using resonance Raman spectroscopy combined with quantum density functional theory calculations. DFT calculations predict that charge remains localized on the P atom, while distributed in the N case. The $\omega_{G'_{Pris}} - \omega_{G'_D}$ frequency splitting between the two peaks of the G′ band in the P-doped SWNTs is smaller than the $\omega_{G'_{Pris}} - \omega_{G'_D}$ for N-doped samples, thus confirming a smaller charge induced perturbation around the defect in the case of P, as compared to the N doping case. This difference between the observed $\omega_{G'_{Pris}} - \omega_{G'_D}$ splitting for different atoms in SWNTs can then be used to explore their doping nature in more detail, beyond the p- or n-type doping identification reported in ref 15. The changes in the RBM and in the $I_{G'_D}/I_{G'_{Pris}}$ indicate that substitutional P doping is more efficient above 0.15 wt % TPP in the precursor solution. Frequency shifts up to -16 cm^{-1} in the tangential (G^+) band of the different P-doped samples are observed only by measuring them with high laser powers, thus indicating that the substitutional P doping enhances the thermal conductivity of bundled SWNT samples. Therefore, as nanotube vibrational properties are sensitive to laser power, care should be taken when analyzing the Raman spectra. DFT calculations also predict that the formation energy for P-doped sites is lower as the curvature increases, thus making narrow diameter nanotubes preferable when compared to large diameter nanotubes, in agreement with the RBM measurements.

Acknowledgment. The authors thank M. S. Dresselhaus for helpful discussions. I.O.M., M.A.P., and A.J. acknowledge financial support from FAPEMIG, *Rede Nacional de Pesquisa em Nanotubos de Carbono*, *Rede National de SPM*, *Instituto de Nanotecnologia* (MCT-CNPq), and CAPES/DAAD-Probral. M.T, H.T., and J.C.-D. acknowledge financial support from CONACYT-Mexico Grants No. 56787 (Laboratory for Nanoscience and Nanotechnology Research-LINAN), 45762 (H.T.), 45772 (M.T.), Fondo Mixto de San Luis Potosí 63001 S-3908 (M.T.), 2004-01-013/SALUD-CONACYT (M.T.), Fondo Mixto de San Luis Potosí 63072 S-3909 (H.T.), 58899-Inter American Collaboration, and PhD scholarship (J.C.D.). E.C.-S., B.G.S., and V.M. acknowledge support by the Division of Materials Science and Engineering, U.S. Department of Energy and by the Center for Nanophase Materials Sciences (CNMS), sponsored by the Division of Scientific User Facilities, U.S. Department of Energy. Computations were performed using the resources of the ORNL institutional cluster and also from the National Energy Research Scientific Computing Center at LBNL.

References

(1) Treacy, M. J.; Ebessen, T. W.; Gibson, J. M. *Nature* **1996**, *381*, 678.
(2) Tans, S. J.; Devoret, M. H.; Dai, H.; Tess, A.; Smalley, R. E.; Gerligs, L. J.; Dekker, C. *Nature* **1997**, *386*, 474.
(3) Tans, S. J.; Verschueren, A. R. M.; Dekker, C. *Nature* **1998**, *393*, 49.
(4) Terrones, M.; Souza Filho, A. G.; Rao, A. M. Doped Carbon Nanotubes: Synthesis, Characterization and Applications. In *Carbon Nanotubes: Advanced Topics in the Synthesis, Structure, Properties*

and Applications; Jorio, A., Dresselhaus, M. S., Dresselhaus, G., Eds.; Springer Series in Topics in Applied Physics 111; Springer-Verlag: Berlin, 2008; pp 531−566.
(5) Gai, P. L.; Stephan, O.; McGuire, K.; Rao, A. M.; Dresselhaus, M. S.; Dresselhaus, G.; Colliex, C. *J. Mater. Chem.* **2004**, *14*, 669.
(6) Villapando-Paez, F.; Zamudio, A.; Elias, A. L.; Son, H.; Barros, E. B.; Chow, S. G.; Kim, Y. A.; Muramatsu, H.; Hayashi, T.; Kong, J.; Terrones, H.; Dresselhaus, G.; Endo, M.; Terrones, M.; Dresselhaus, M. S. *Chem. Phys. Lett.* **2006**, *424*, 345.
(7) McGuire, K.; Gothard, N.; Gai, P. L.; Dresselhaus, M. S.; Sumanasekera, G.; Rao, A. M. *Carbon* **2005**, *43*, 219.
(8) Sumpter, B. G.; Meunier, V.; Romo-Herrera, J. M.; Cruz-Silva, E.; Cullen, D. A.; Terrones, H.; Smith, D. J.; Terrones, M. *ACS Nano* **2007**, *1*, 369.
(9) Cruz-Silva, E.; Cullen, D. A.; Gu, L.; Romo-Herrera, J. M.; Muoz-Sandoval, E.; Lpez-Uras, F.; Sumpter, B. G.; Meunier, V.; Charlier, J.-C.; Smith, D. J.; Terrones, H.; Terrones, M. *ACS Nano* **2008**, *2*, 441.
(10) Jourdain, V.; Kanzow, H.; Castingloles, M.; Loiseau, A.; Bernier, P. *Chem. Phys. Lett.* **2002**, *364*, 27.
(11) Jourdain, V.; Stéphan, O.; Castingloles, M.; Loiseau, A.; Bernier, P. *Adv. Mater.* **2004**, *16*, 447.
(12) Jourdain, V.; Palillet, M.; Almairac, R.; Loiseau, A.; Bernier, P. *J. Phys. Chem. B* **2005**, *109*, 1380.
(13) Zhang, J.; Liu, X.; Blume, R.; Zhang, A.; Schlögl, R.; Su, D. S. *Science* **2008**, *322*, 73.
(14) Ewels, C. P.; Cheikh, H. E.; Suarez-Martinez, I.; Van Lier, G. *Phys. Chem. Chem. Phys.* **2008**, *10*, 2145.
(15) Maciel, I. O.; Anderson, N.; Pimenta, M. A.; Hartschuh, A.; Qian, H.; Terrones, M.; Terrones, H.; Campos-Delgado, J.; Rao, A. M.; Novotny, L.; Jorio, A. *Nat. Mater.* **2008**, *7*, 878.
(16) Soler, J. M.; Artacho, E.; Gale, J. D.; García, A.; Junquera, J.; Ordejón, P.; Sánchez-Portal, D. *J. Phys.: Condens. Matter* **2002**, *14*, 2745.
(17) Kane, B. E. *Nature (London)* **1998**, *393*, 133.
(18) Koiller, B.; Hu, X.; Das Sarma, S. *Phys. Rev. Lett.* **2002**, *88*, 027903.
(19) Souza Filho, A. G.; Jorio, A.; Samsonidze, Ge. G.; Dresselhaus, G.; Pimenta, M. A.; Dresselhaus, M. S.; Swan, Anna K.; Ünlü, M. S.; Goldberg, B. B.; Saito, R. *Phys. Rev. B* **2003**, *67*, 035427.
(20) Saito, R.; Fantini, C.; Jiang, J. Excitonic States and Resonance Raman Spectroscopy of Single-Wall Carbon Nanotubes. In *Carbon Nanotubes: Advanced Topics in the Synthesis, Structure, Properties and Applications*; Jorio, A., Dresselhaus, M. S., Dresselhaus, G., Eds.; Springer Series in Topics in Applied Physics 111; Springer-Verlag: Berlin, 2008; pp 251−285.
(21) Maciel, I. O.; Pimenta, M. A.; Terrones, M.; Terrones, H.; Campos-Delgado, J.; Jorio, A. *Phys. Status Solidi B* **2008**, *245*, 2197.
(22) Araujo, P. T.; Maciel, I. O.; Pesce, P. B. C.; Pimenta, M. A.; Doorn, S. K.; Qian, H.; Hartschuh, A.; Steiner, M.; Grigorian, L.; Hata, K.; Jorio, A. *Phys. Rev. B* **2008**, *77*, 241403R.
(23) Fantini, C.; Jorio, A.; Souza, M.; Strano, M. S.; Dresselhaus, M. S.; Pimenta, M. A. *Phys. Rev. Lett.* **2004**, *93*, 147406.
(24) Telg, H.; Maultzsch, J.; Reich, S.; Hennrich, F.; Thomsen, C. *Phys. Rev. Lett.* **2004**, *93*, 177401.
(25) O'Connell, M. J.; Sivaram, S.; Doorn, S. K. *Phys. Rev. B* **2004**, *69*, 235415.
(26) Araujo, P. T.; Doorn, S. K.; Kilina, S.; Tretiak, S.; Einarsson, E.; Maruyama, S.; Chacham, H.; Pimenta, M. A.; Jorio, A. *Phys. Rev. Lett.* **2007**, *98*, 067401.
(27) Popov, V. N.; Henrard, L.; Lambin, P. *Phys. Rev. B* **2005**, *72*, 035436.
(28) Machón, M.; Reich, S.; Thomsen, C. *Phys. Rev. B* **2006**, *74*, 205423.
(29) Jiang, J.; Saito, R.; Samsonidze, Ge. G.; Jorio, A.; Chou, S. G.; Dresselhaus, G.; Dresselhaus, M. S. *Phys. Rev. B* **2007**, *75*, 035405.
(30) Tsang, J. C.; Freitag, M.; Perebeinos, V.; Liu, J.; Avouris, P. *Nat. Nanotechnol.* **2007**, *2*, 725.
(31) Rao, A. M.; Eklund, P. C.; Bandow, S.; Thess, A.; Smalley, R. E. *Nature* **1997**, *388*, 257.
(32) Souza, A. G.; Jorio, A.; Samsonidze, Ge. G.; Dresselhaus, G.; Sato, R.; Dresselhaus, M. S. *Nanotechnology* **2003**, *14*, 1130.

NL9004207